

Seismic Inversion and Self-Organizing Maps (SOM) for Facies Characterization in Faulted Clastic Reservoirs: A Case Study from the Poseidon Field, Western Australia

Elena Veliz¹, Elise Masse¹, Romain Baillet¹, Arnaud Fournillon¹, and Cristian Zura²

Search and Discovery Article #42614 (2026)**

Posted February 25, 2026

*Adapted from extended abstract based on oral presentation given at AAPG International Conference and Exhibition (ICE) Rio de Janeiro, 30 September - 3 October, 2025.

**Datapages © 2026. Serial rights given by author. For all other rights contact author directly. DOI:10.1306/42614Veliz2026

¹Beicip-Franlab

²Universidad Central del Ecuador

Abstract

This study presents a workflow for seismic inversion and characterization using both unsupervised and supervised Self-Organizing Maps (SOM) to analyze a clastic faulted and tilted reservoir in the Poseidon field, Western Australia. The aim is to delineate lithology, especially the porous sands, in a complex geological setting, benchmarking this brand-new characterization approach with traditional statistical methods, after seismic inversion. The SOM is powerful to handle large datasets, recognize outliers, and preserve the relationships between data ensures accurate and reliable reservoir characterization, even in challenging, data-scarce areas. In this case study, one full-stack, three angle-stacks, and eight wells, are available to study the Plover and Montara Formations. The Plover Formation is characterized by fluvio-deltaic sands and volcanic materials, while the Montara Formation comprises deltaic to shallow marine deposits (ConocoPhillips, 2012).

A Residual Normal Moveout (RNMO) correction has been applied to ensure the compatibility between the stacks before any inversion process. After controlling and conditioning the well database, the wavelets have been extracted statistically and optimized in phase and energy using a multi-trace, multi-well approach. The well tie has been carried out using all the stacks simultaneously, ensuring good control while interpolating the impedances along correlation lines for the prior model building. The model-based elastic inversion parameter set has been designed to ensure a relatively high convergence, incorporating the seismic signal and removing the noise, partly thanks to its grid-based aspect, and a prior dip volume estimated from seismic data.

A petro-elastic model has been built, both at a well scale and after upscaling, providing various training and validation datasets for the SOM. If compatible, these datasets are then enriched using more seismic attributes. The characterization process included both unsupervised and supervised SOM applied to the inversion results and attributes, in 3D. The unsupervised SOM reorganizes these high-dimensional data into a two-dimensional map, to visually select features related to key lithologies, enhancing both geological interpretability and control. The supervised SOM automatizes the key neurons selection, producing a labeled cube with lithological classes. After adjusting key parameters and inputs in both steps, the lithologies tend to be better identified, especially the sands, and, to a lesser extent, the volcanic materials, compared to classical statistical methods such as the discriminant analysis.

Quality controls based on geological criteria were crucial for validating the results, with visual inspections confirming that the key neuron selection correspond to realistic geological features such as channels, fluvial deltas, and sand deposits such as barrier fringing sandstones. This workflow, combining advanced seismic inversion techniques, machine learning algorithms, and rigorous quality control mixing machine learning and geological concepts, demonstrates the potential to effectively characterize complex reservoirs, even in challenging geological conditions.

Introduction

Characterizing reservoirs in structurally complex clastic settings requires approaches capable of integrating geological understanding with advanced geophysical and machine-learning techniques. The Poseidon Field, located in the Browse Basin offshore Western Australia, provides a challenging case study due to its tectonic evolution during Early to Middle Jurassic rifting ([Figure 1](#)), which produced half-graben geometries, major normal faults, and significant stratigraphic compartmentalization (Struckmeyer et al., 1998). The reservoir interval, comprising the Montara and Plover formations, includes fluvial, tidal, and shallow-marine sandstones interbedded with shales, carbonates, and volcanic facies (Kuske et al., 2015, Tovagliari & George, 2014). Such heterogeneity, combined with faulting and tilting, complicates lithological prediction and reservoir modeling, and therefore, is a perfect playground to apply an inversion and advanced quantitative interpretation study. The objective is to improve facies characterization, particularly the identification of sandstones, through an integrated workflow using sequentially unsupervised, then supervised Self-Organizing Maps (SOM) (Gardashli et al., 2025). The approach is evaluated and validated using independent geological and structural evidence.

Methodology

The workflow begins with a comprehensive pre-processing stage involving one full-stack seismic volume, three angle stacks, interpreted horizons, and eight wells. Residual Normal Moveout correction was applied to ensure consistency between stacks, followed by multi-trace, multi-well wavelet extraction to optimize both phase and energy. Simultaneous well ties across all stacks enabled consistent impedance interpolation for prior model infilling. Petro-elastic modeling was performed at both log and upscaled seismic scales, generating datasets for training and validating machine-learning algorithms.

A model-based elastic inversion algorithm was selected to maximize seismic bandwidth while minimizing random noise. Convergence analysis demonstrated that the cost function reaches a plateau at 90.8%, with rejected discrepancies attributed to noise during early-stage signal analysis. Residual and energy-ratio diagnostics confirmed the stability of the inversion across partial stacks, and inverted impedance curves showed strong agreement with measured well logs. The resulting optimized properties captured key lateral and vertical contrasts, possibly influenced by the structure, as shown in [Figure 2](#). This technique was decisive to unveil and quantify changes in the reservoir, since impedance responds to lithological variations and therefore provides valuable input for reservoir characterization methods. The black arrows on the sections highlight the increase of values of P-impedance, S-impedance, and the low values of density around the Plover reservoir. The advantages of elastic

inversion rely not only on detecting properties but also on reducing significantly the random noise in the synthetic data, providing a reliable seismic to use. The density, poorly updated using conventional seismic data, has been discarded from the seismic characterization analysis.

The Self-Organizing Maps (SOM) algorithm introduced by Kohonen (1998) was applied in two complementary modes, both applied sequentially, as illustrated in [Figure 3](#). The unsupervised SOM organizes high-dimensional inversion attributes into two-dimensional neuron maps, revealing natural clusters and unlabeled facies patterns. This step requires a set of dedicated QCs, using key metrics, such as the *quantization error*, associated to the good match between the neurons and the data, and the *topographic error*, checking the lateral consistency of patterns in the topography space. The supervised SOM, built upon the unsupervised SOM, incorporated petro-elastic models and well-based facies interpretations, enabling the algorithm to map lithological signatures onto the typical attribute responses. Preliminary upscaled logs and attribute cross plots confirmed the separability of key facies, particularly porous sandstones, and the supervised SOM ultimately produced a robust classifier of the attributes to the different lithologies, associated with scores, distinguishing sandstones, shales, volcanics, and carbonates, which consistency was controlled both using topology view and confusion matrix. This classification was then propagated in 3D, providing a labeled 3D lithology cube for further analysis.

Application to Poseidon dataset

The workflow was applied to Montara and Plover formations, where the reservoir identification is challenging due to structural complexity and facies heterogeneity. Preliminarily to the SOM application, to identify trends in the data, a petro-elastic model was designed to capture the relationships between P-impedance and S-impedance while incorporating lithological information. At the well scale, distinct trends can be observed across the crossplots. Volcanic facies exhibit a wide range of values, indicating the presence of at least two volcanic types characterized by low and high impedances. After a seismic upscaling mimicking the seismic resolution, despite the significant reduction of samples, the main cluster trends remain recognizable ([Figure 4](#)). This filtering step was applied to ensure consistency between the training data and the seismic-frequency data used for labeling. Additionally, in the P-impedance versus VP/VS domain, target sand facies show a clear cutoff in VP/VS values. To identify the lithology, P-impedance, S-impedance and VP/VS were then selected as input for the SOM methodology. The petro-elastic model was stored to train the lithology classifier, during the supervised SOM step.

The unsupervised SOM provided an exploratory view of lithological variability, highlighting lateral changes and potential stratigraphic trends without imposing predefined labels. In [Figure 5](#), neuron maps represent the zonation of key patterns, where identical neuron positions correspond to similar combinations of elastic properties—for example, increases in P-impedance and S-impedance associated with a decrease in V_p/V_s .

Multiple parameter configurations were tested during several iterations of the workflow. Grid size, normalization methods, and the number of iterations were evaluated using algorithm performance metrics and a topology visualization tool. Dealing with true elastic properties allows us to easily link these machine learning visuals with traditional petro-elastic analysis. Variations in these parameters mainly affected clusters with smaller proportions, while the dominant patterns remained stable and recognizable. To simplify, as a first run, the interpretation of the classes, a class reduction step from hundred (100) to eight (8) classes using K-means clustering was applied ([Figure 6](#)). This approach proved effective in

identifying zones of interest and in guiding the subsequent supervised classification. Indeed, it can be observed that typical responses are distributed stratigraphically; the red class could correspond to the volcanic samples, comparing with the well data.

As a second step of the workflow, sequentially with the unsupervised analysis, the supervised SOM allowed another automatic labelling to reduce the classes from hundred (100) to four (4), produced a detailed lithology cube including shale (green), sand (yellow), carbonates (blue) and volcanics (pink) that shows strong agreement with well observations, as illustrated in [Figure 7](#). The predicted facies closely match the measured lithologies along the Boreas-1 well trajectory, particularly for sandstones and shales, which are critical for reservoir quality assessment. It is interesting to highlight that the volcanic facies were preferentially detected in the Montara formation, in adequation with the unsupervised class highlighted in red [Figure 6](#). To validate the predictions, a cross plot of samples extracted along the well trajectory was analyzed [Figure 7](#), demonstrating trends consistent with those observed in the original well logs. It can be observed that the limits between the facies are easily visible, but not strict, as VP/VS attribute was also involved in the classification.

[Figure 9](#) presents confusion matrix, illustrating the mutual consistency between initial and predicted facies, expressed as the percentage of restitution. Higher compatibility values (blue) indicate higher confidence in facies classification. Sands and shales show the highest levels of agreement, while volcanics and carbonates exhibit lower compatibility. This reduced performance is likely due to overlapping elastic signatures with other facies in the selected attribute space, which complicates discrimination and introduces additional uncertainty for these lithologies.

To further validate the results, structural attributes such as similarity, guided similarity, and dip-derived attribute were analyzed using an unsupervised SOM, generating a 3D structural volume that delineated fault networks with high clarity. Integrating this structural information with the facies cube provided a coherent geological interpretation in which predicted facies geometries aligned with depositional trends inferred from paleogeographic reconstructions (Tovagliari, 2013). Channel orientations and sandstone bodies corresponded to paleocurrent directions observed in borehole image logs, reinforcing the geological plausibility of the machine-learning outputs ([Figure 10](#)).

Conclusions

The combination of elastic seismic inversion and Self-Organizing Maps offers a powerful workflow for reservoir characterization in faulted and heterogeneous clastic systems. The inversion provided impedance volumes that reduced uncertainty in areas with strong lateral and thickness variations, while SOM enabled both exploratory clustering and supervised lithological classification. The resulting facies predictions were not only internally consistent but also aligned with independent geological and structural evidence, demonstrating that the machine-learning outputs captured meaningful petro-elastic and geological trends rather than purely mathematical patterns. Applied to the Poseidon Field, this integrated approach improved the identification of porous sandstones and volcanic facies and outperformed traditional statistical methods. The workflow provides a robust and geologically grounded methodology with significant implications for exploration and development in similarly complex tectonic and depositional environments.

Acknowledgments

The authors gratefully acknowledge Geoscience Australia and ConocoPhillips for providing the open-source data used in this study.

References

ConocoPhillips (2012). (Browse Basin) Pty Ltd, WA-315-P y WA-398-P Browse Basin Western Australia 2009 Poseidon 3D Marine Surface Seismic Survey Interpretation Report

ConocoPhillips (2011). (Browse Basin) Poseidon field Well reports.

Gardashli, T., Baillet, R., Desgoutte, N. (2025). Application of a semi-supervised Self-Organizing Map algorithm for seismic facies classification using inversion attributes. IMAGE Conference 2025. Houston, Texas, United States.

Kohonen, T. (1998). The self-organizing map. *Neurocomputing*, 21(1-3), 1–6. [https://doi.org/10.1016/s0925-2312\(98\)00030-7](https://doi.org/10.1016/s0925-2312(98)00030-7)

Kuske, T., Ie Poidevin, S. & Edwards, D. (2015). Browse Basin petroleum accumulations. *The APPEA Journal*, 55(2), 463–463. <https://doi.org/10.1071/aj14098>

Struckmeyer, H.I.M., Blevin, J.E., Sayers, J., Totterdell, J.M., Baxter, K. & Cathro, D.L. (1998). Structural evolution of the Browse Basin, Northwest Shelf: New concepts from deep-seismic data. *The sedimentary basins of Western Australia 2: Proceedings of the Petroleum Exploration Society of Australia Symposium, Perth*, 345-367.

Tovagliari, F. (2013). Depositional history and paleogeography of the Jurassic Plover Formation in Calliance and Brecknock fields, Browse Basin, North West Shelf, Australia. *Doctoral thesis*.

Tovagliari, F. & George, AD. (2014) Stratigraphic architecture of an Early Middle Jurassic tidally influenced deltaic system (Plover Formation), Browse Basin, Australian Northwest Shelf. *Mar Pet Geol* 49:59–83.

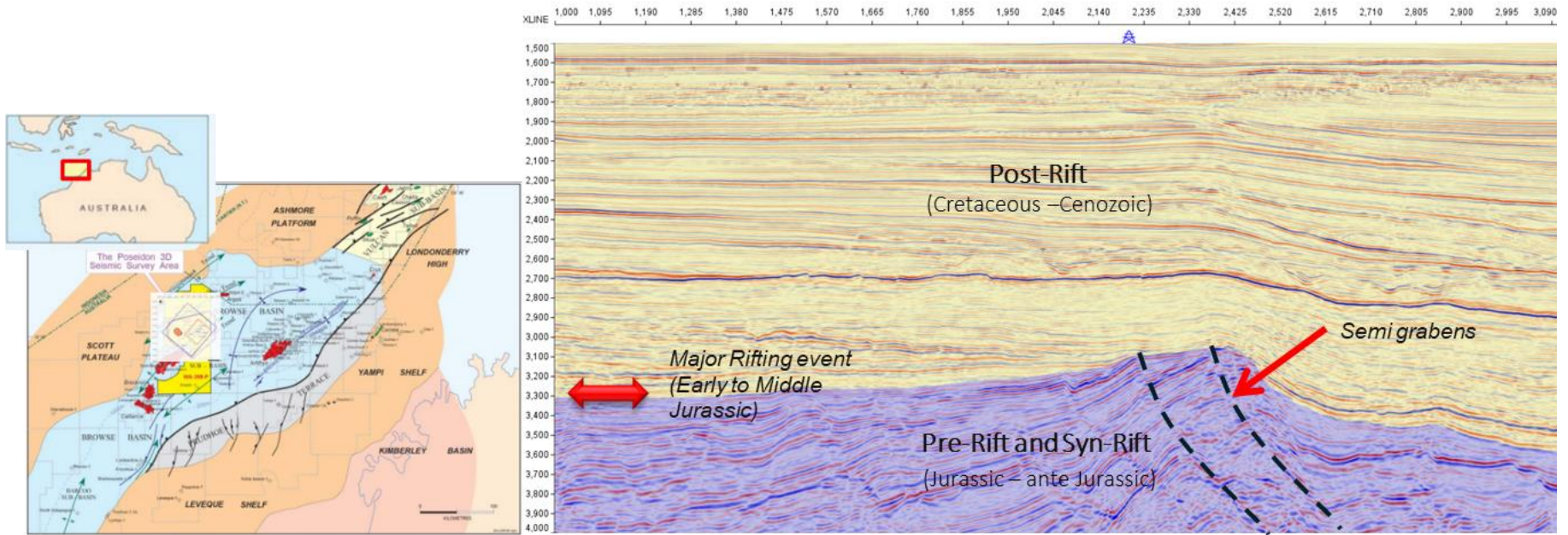


Figure 1. Left: Location map of the Browse basin and its limits, highlighting the area of the Poseidon field. Modified from ConocoPhillips, 2012. Right: Representative seismic section identifying the Jurassic Major Rifting and the Post-Rift and Pre-Rift-Syn-Rift

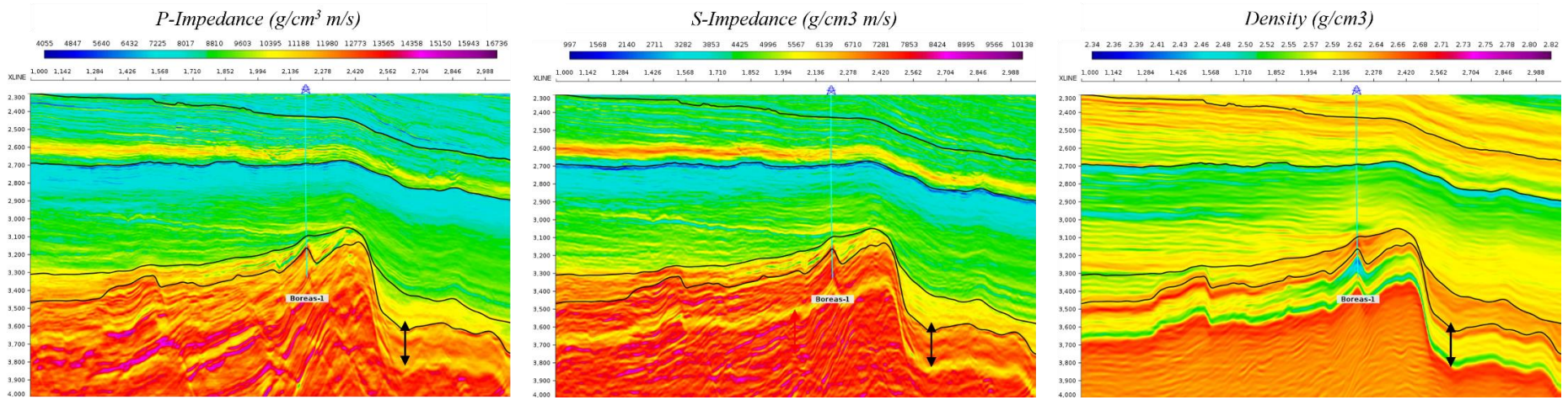
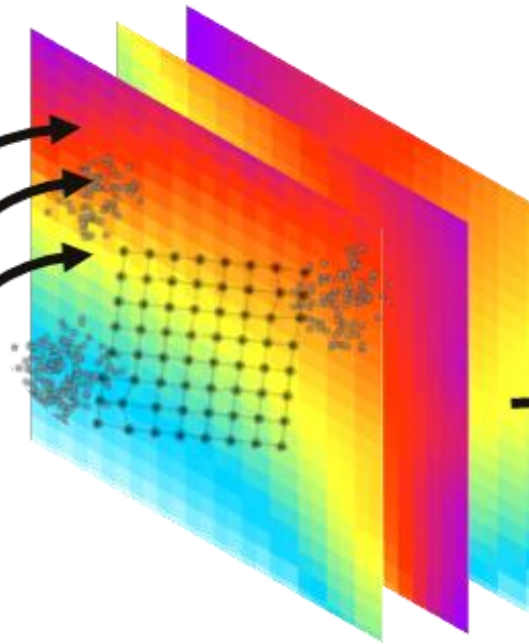
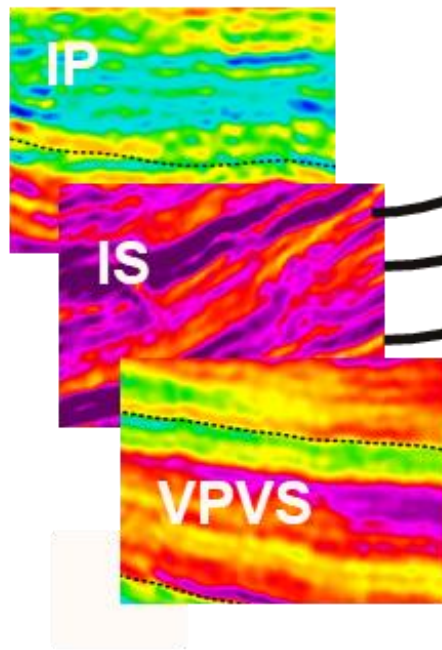


Figure 2. Results of the elastic seismic inversion. From left to right: P-impedance, S-impedance and Density.

High-dimensional data

- *Seismic attributes*
- *Inversion results*



Map of neurons

The neurons compete between each other to best represent the input samples.

Low-dimensional
unbiased
interpretable map

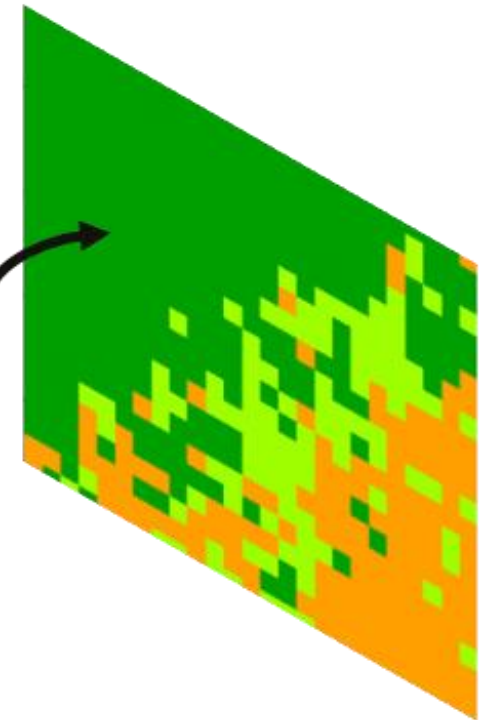


Figure 3. Scheme of the Self-Organizing Maps technique. Flattening and prediction phases are illustrated on the map of neurons and interpretable map (respectively).

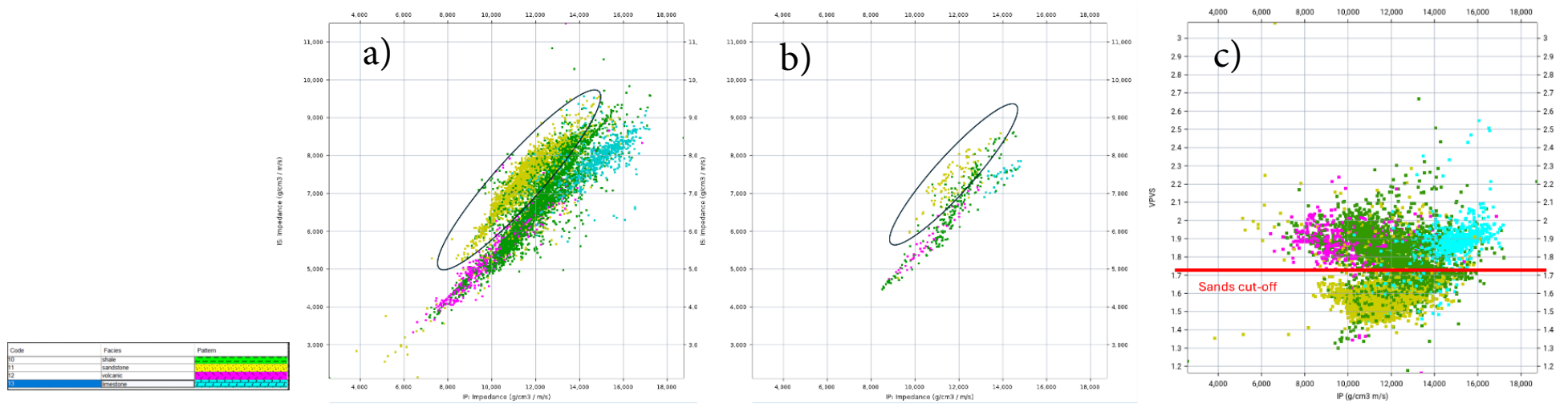


Figure 4. Petro-elastic models cross plots (a) P-impedance vs. S-impedance at well scale. (b) P-impedance vs. S-impedance at seismic scale. (c) P-impedance vs. VPVS at well scale.

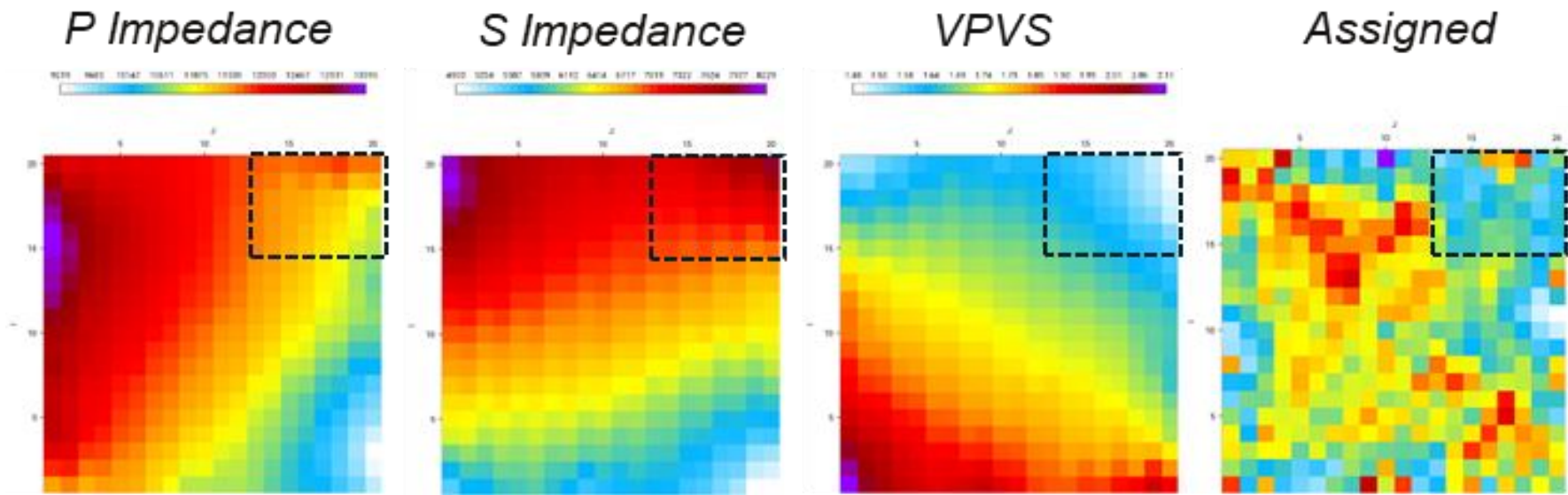


Figure 5. Maps of each attribute used for the un-supervised approach in the neuron grid: P-impedance ($\text{g/cm}^3 / \text{m/s}$), S-impedance ($\text{g/cm}^3 / \text{m/s}$) and VPVS ratio (no unit). Note that on the upper right corner, the values of P and S impedances increase while the VPVS decreases on the same assigned neurons. In this method, the attribute changes are gradual, and therefore, close typical response (in the neuron grid) should correspond to similar facies, facilitating the interpretation.

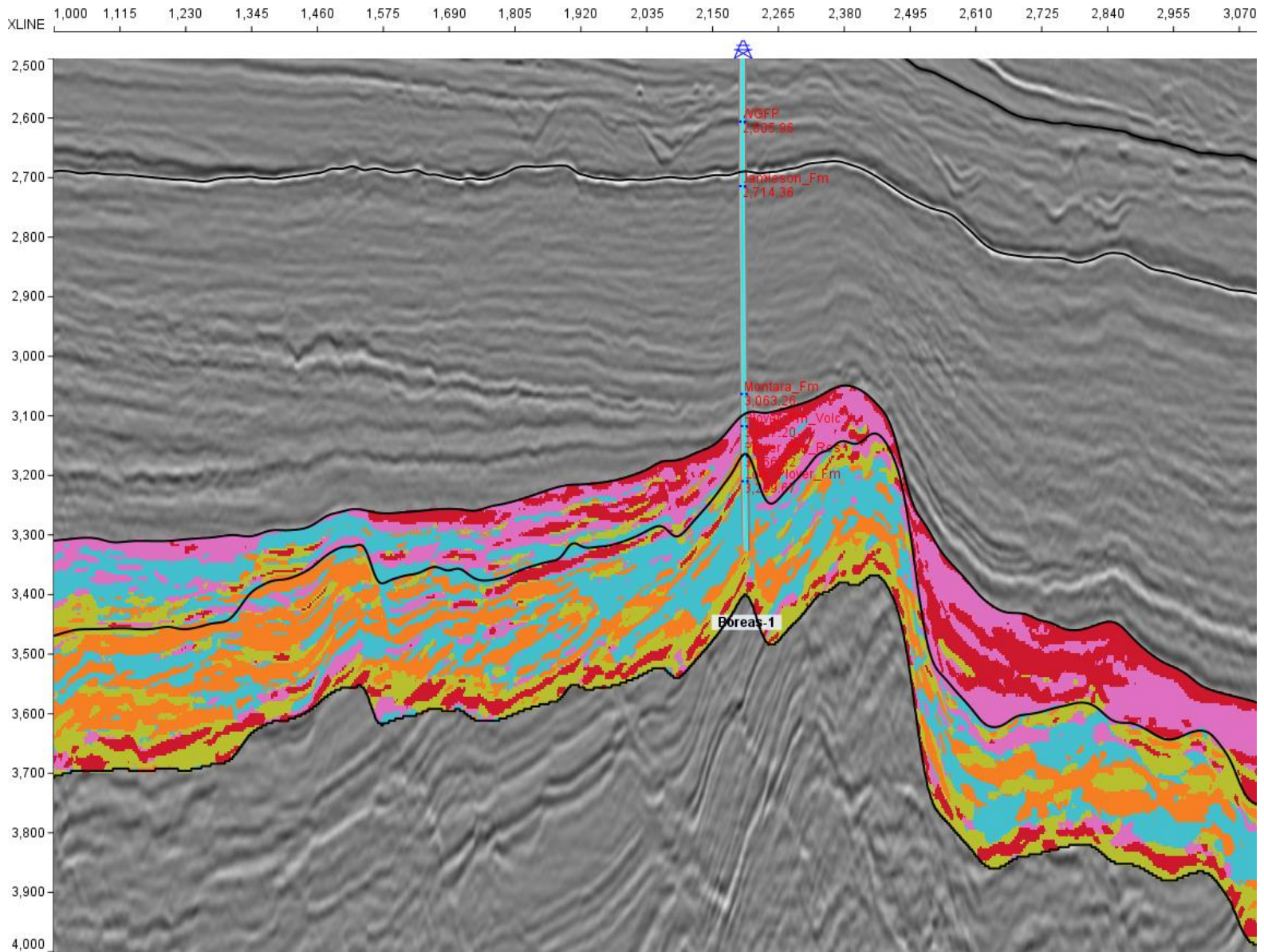


Figure 6. Seismic section showing the clusters of facies obtained using an un-supervised SOM and having applied a K-means reduction.

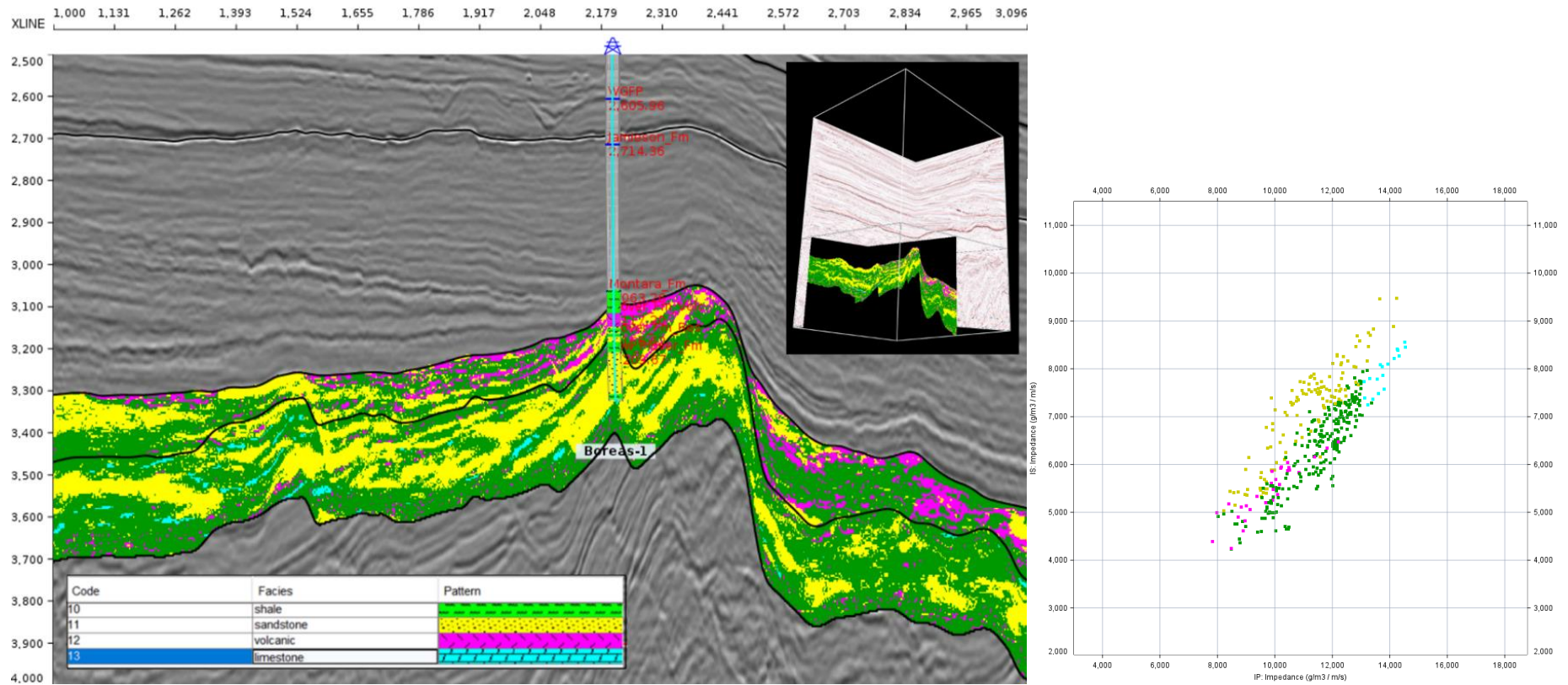


Figure 7. Seismic section (left) with a superposition of the predicted facies in the interval of interest using the semi-supervised SOM. The section intersects Boreas-1. Cross plot P-impedance vs. S-impedance (right). The samples correspond to the extraction at the trajectory of the well in the volume of predicted facies.

	Predicted 10	Predicted 11	Predicted 12	Predicted 13
Actual 10	62.204%	11.241%	11.715%	14.84%
Actual 11	10.609%	83.478%	1.913%	4%
Actual 12	44.444%	2.293%	50.088%	3.175%
Actual 13	10.057%	6.374%	0%	83.569%

	Predicted 10	Predicted 11	Predicted 12	Predicted 13
Actual 10	81.506%	21.199%	56.988%	44.003%
Actual 11	6.689%	75.75%	4.478%	5.707%
Actual 12	9.211%	0.684%	38.535%	1.489%
Actual 13	2.595%	2.367%	0%	48.801%

Figure 9. Restitution tables (left) Initial facies consistent with predicted facies (right) Predicted facies consistent with initial facies. Codification: shale (10), sand (11), volcanic (12), carbonates (13). A high score in both tables indicates a good prediction, while a good score only on the left table or on the right table would indicate either an overestimation or underestimation, respectively. The predicted volcanic samples and carbonate samples are slightly overestimated and mostly mixed with shales. The sand samples are very well restituted.

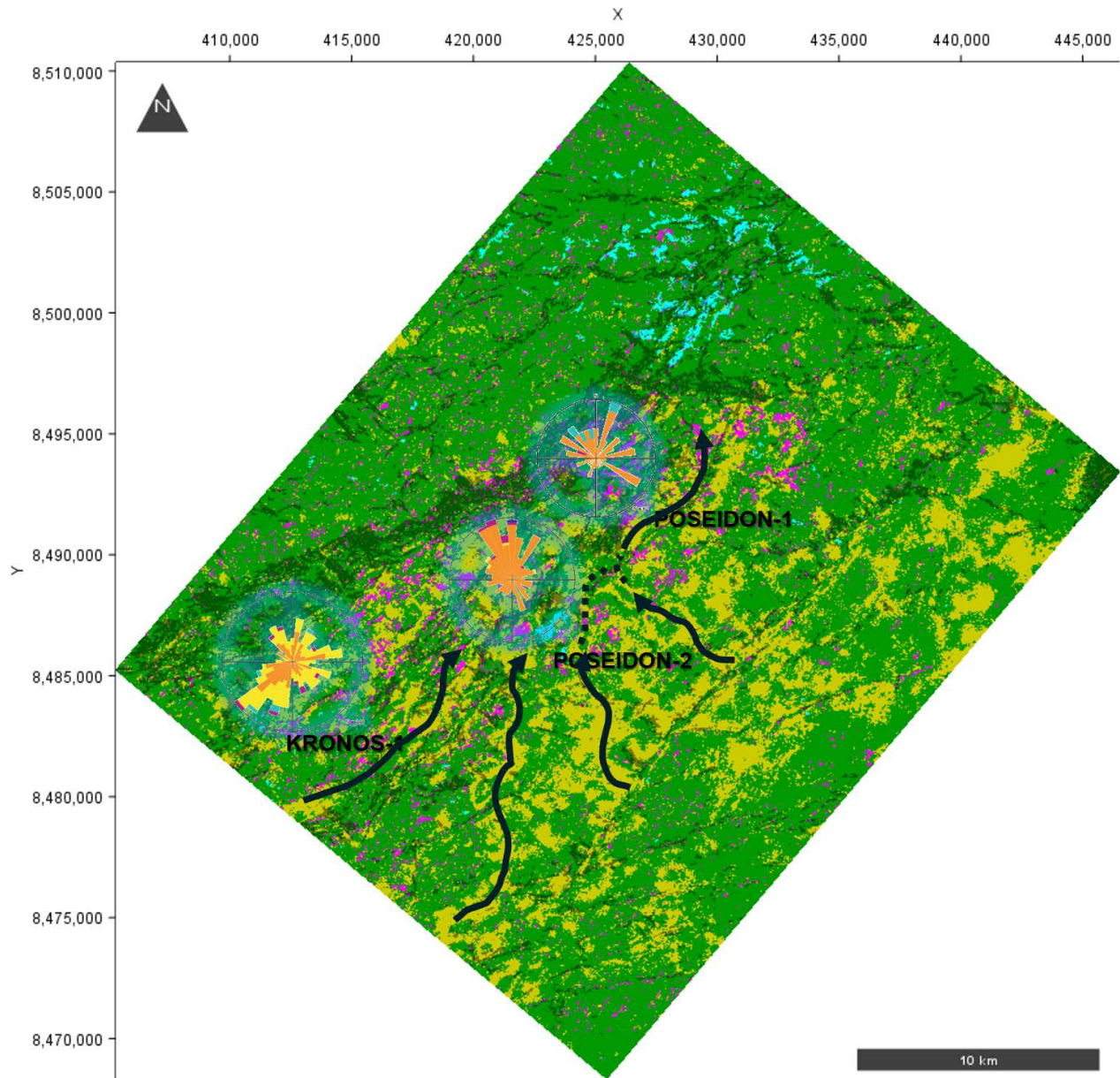


Figure 10. Map extraction at reservoir interval showing the distribution of facies, the structural network and superposed, the interpreted paleocurrents and BHI diagrams. Modified from: ConocoPhillips, 2011.